Synthesis, Structure, and Characterisation of a New Phenolato-Bridged Manganese Complex $[Mn_2(mL)_2]^{2+}$: Chemical and Electrochemical Access to a New Mono-μ-Oxo Dimanganese Core Unit

Christelle Hureau,[a] Laurent Sabater,[a] Elodie Anxolabéhère-Mallart,*[a] Martine Nierlich,[b] Marie-France Charlot,[a] Florence Gonnet,[c] Eric Rivière,[a] and Geneviève Blondin*[a]

Abstract: The dinuclear phenolato-bridged complex $[(mL)Mn^{II}Mn^{II}(mL)](ClO_4)_2$ (**1**$(ClO_4)_2$) has been obtained with the new $[N_4O]$ pentadentate ligand mL^- (mLH = *N*,*N*′-bis-(2-pyridylmethyl)-*N*-(2-hydroxybenzyl)-*N*′-methyl-ethane-1,2-diamine) and has been characterised by X-ray crystallography. X- and Q-band EPR spectra were recorded and their variation with temperature was examined. All spectra exhibit features extending over 0–800 mT at the X band and over 100–1450 mT at the Q band, features that are usually observed for dinuclear Mn^{II} complexes. Cyclic voltammetry of **1** exhibits two irreversible oxidation waves at $E_1^p = 0.89$ V and $E_2^p = 1.02$ V, accompanied on the reverse scan by an ill-defined cathodic wave at $E_{1'}^p = 0.56$ V (all measured versus the saturated calomel electrode (SCE)). Upon chemical oxidation with *t*BuOOH (10 equiv) at 20 °C, **1** is transformed into the mono-μ-oxo species $[(mL)Mn^{III}(\mu\text{-}O)Mn^{III}(mL)]^{2+}$ (**2**), which eventually partially evolves into the di-μ-oxo species $[(mL)Mn^{III}(\mu\text{-}O)_2Mn^{IV}(mL)]^{n+}$ (**3**) in which one of the aromatic rings of the ligand is decoordinated. The UV/Vis spectrum of **2** displays a large absorption band at 507 nm, which is attributed to a phenolate→Mn^{III} charge-transfer transition. The cyclovoltammogram of **2** exhibits two reversible oxidation waves, at 0.65 and 1.16 V versus the SCE, corresponding to the $Mn^{III}Mn^{III}$/$Mn^{III}Mn^{IV}$ and $Mn^{III}Mn^{IV}$/$Mn^{IV}Mn^{IV}$ oxidation processes, respectively. The one-electron electrochemical oxidation of **2** leads to the mono-μ-oxo mixed-valent species $[(mL)Mn^{III}(\mu\text{-}O)Mn^{IV}(mL)]^{3+}$ (**2ox**). The UV/Vis spectrum of **2ox** exhibits one large band at 643 nm, which is attributed to the phenolate→Mn^{IV} charge-transfer transition. **2ox** can also be obtained by the direct electrochemical oxidation of **1** in the presence of an external base. The **2ox** and **3** species exhibit a 16-line EPR signal with first peak to last trough widths of 125 and 111 mT, respectively. Both spectra have been simulated by using colinear rhombic Mn-hyperfine tensors. Mechanisms for the chemical formation of **2** and the electrochemical oxidation of **1** into **2ox** are proposed.

Keywords: electrochemistry · EPR spectroscopy · manganese · N,O ligands · oxidation

Introduction

The involvement of manganese in several biological systems and processes is now well-known.[1,2] For example, manganese dinuclear sites are present in metalloproteins such as manganese catalase,[3,4] arginase[5] and ribonucleotide reductase.[6] Another very important biological system is the tetranuclear Mn–oxo cluster, a key element of the OEC[7] located in photosystem II of green plants,[8–12] which catalyses the light-induced oxidation of water into dioxygen.

A photo-induced electron abstraction from the OEC occurs during each of the four transition states of the catalytic cycle (S_0–S_4 of the Kok cycle).[13] Crystal structures of the *Synechococcus elongatus* photosystem-II dark-adapted S_1 state at 3.8 Å resolution[14] and of the *Thermosynechococ-*

[a] C. Hureau, L. Sabater, E. Anxolabéhère-Mallart, M.-F. Charlot, E. Rivière, G. Blondin
Laboratoire de Chimie Inorganique, UMR 8613, LRC-CEA n°33 V
Institut de Chimie Moléculaire et des Matériaux d'Orsay
Université Paris-Sud, 91405 Orsay Cedex (France)
Fax: (+33) 1-69-15-47-54
E-mail: eanxolab@icmo.u-psud.fr
gblondin@icmo.u-psud.fr

[b] M. Nierlich
CEA Saclay, DRECAM/SCM Bat 125
91191 Gif-sur-Yvette (France)

[c] F. Gonnet
Laboratoire Analyse et Environnement, UMR 8587
Bâtiment des Sciences, Université d'Evry Val d'Essonne
Boulevard François Mitterrand, 91025 Evry Cedex (France)

Supporting information for this article is available on the WWW under http://www.chemeurj.org/ or from the author.

DOI: 10.1002/chem.200305515

cus vulcanus photosystem II at 3.7 Å resolution[15] have been reported, but the spatial arrangement of the Mn ions and the nature of the oxygenated bridges have not been resolved yet.[16] Information on the structure and valence of the Mn cluster has mainly been obtained from X-ray absorption[9,12,17,18] and EPR studies.[19–22] Comparison with the spectroscopic signatures of a wide variety of manganese compounds was of crucial importance. As a consequence of unresolved structural details, designing biological manganese models is still a challenge for inorganic chemists, as is the investigation of the spectroscopic characteristics of these compounds. On the basis of EXAFS data[1,23,24] as well as theoretical investigations,[25–29] the Mn cluster has been proposed to be a cluster consisting of at least two di-μ-oxo- and one mono-μ-oxo-bridged Mn moieties. We and other groups have synthesised a large number of high-valent Mn–oxo model complexes with various nitrogeneous ligands and cores.[29–34] The three prevalent core units in this chemistry are the di-μ-oxo [Mn-(μ-O)$_2$-Mn],[35–37] the di-μ-oxo-mono-μ-carboxylato [Mn-(μ-O)$_2$(μ-O$_2$CR)-Mn][38–44] and the mono-μ-oxo-di-μ-acetato [Mn-(μ-O)(μ-OAc)$_2$-Mn] moieties.[43,45–49] However, there are very few examples of the unsupported mono-μ-oxo-bridged [Mn-(μ-O)-Mn] system,[44,50–56] especially in the $Mn^{III}Mn^{IV}$ oxidation state. To our knowledge, only two examples are reported in the literature, one with a porphyrinic ligand[57] and one with a non-porphyrinic pentadentate ligand.[34]

The EPR-active S_2 state of the OEC, generated from the dark-adapted photosystem II by flash illumination at 273 K, shows the well-known multiline EPR signal.[19] This spectrum contains at least 19 Mn-hyperfine lines ($I_{Mn}=5/2$) centred at $g\approx2.0$, which arise from an $S=1/2$ ground state. Based on the data recorded from different spectroscopic techniques derived from X-ray absorption, a general consensus has been reached for an Mn^{III}/Mn^{IV} composition of the OEC in the S_2 state. Attempts to simulate this signal[22,58] and theoretical analysis[59] of the possible spin densities have shown quite unambiguously that all four Mn ions of the oxo cluster must be electronically coupled to each other. A thorough study of the EPR features of $Mn^{III}Mn^{IV}$–oxo dinuclear systems showed that the nature of the oxo core unit finely controls the EPR signature. Subsequently, a detailed multifrequency EPR analysis of dinuclear complexes[36,60–62] has been of great interest in the course of the characterisation of the OEC tetrameric complex. Even at the X band, both [Mn^{III}-(μ-O)$_2$-Mn^{IV}]$^{3+}$[1,33,37,63–65] and [Mn^{III}-(μ-O)$_2$(μ-OAc)-Mn^{IV}]$^{2+}$[42] systems present 125 mT (peak to trough), 16-line spectra that differ in their relative line intensities, while the mono-μ-oxo complex [(L′)Mn^{III}-(μ-O)-Mn^{IV}(L′)]$^{3+}$ (L′H is shown in Scheme 1) by Horner et al.[34] exhibits a 119 mT, 18-line spectrum, with a peculiar distribution of the line intensities.

In order to obtain a new mono-μ-oxo complex, we have designed a ligand, L_aH (Scheme 1), that is very similar to the one used by Horner et al. Nevertheless, as we reported in a previous paper,[66] the synthetic route used for the generation of [(L′)Mn^{III}-(μ-O)-Mn^{IV}(L′)]$^{3+}$ (the reaction of $Mn(OAc)_3\cdot2H_2O$ with the free ligand) did not lead to the formation of the expected mono-μ-oxo complex with the new ligand. Indeed, a 1:1 mixture of two dinuclear phenolato-bridged cations, [(L_i)$Mn^{II}Mn^{II}$(L_i)]$^{2+}$ and [(L_a)$Mn^{II}Mn^{II}$(L_i)]$^{2+}$, was obtained, due to oxidation of the secondary amine group of L_a^- into an imine, the ligand thus becoming L_i^- (L_iH is shown in Scheme 1), with the concomitant reduction of Mn^{III} into Mn^{II}.[66] To avoid such behaviour of the compounds, we have here used a protected ligand, mLH[7] (Scheme 1), where the secondary amine is methylated.

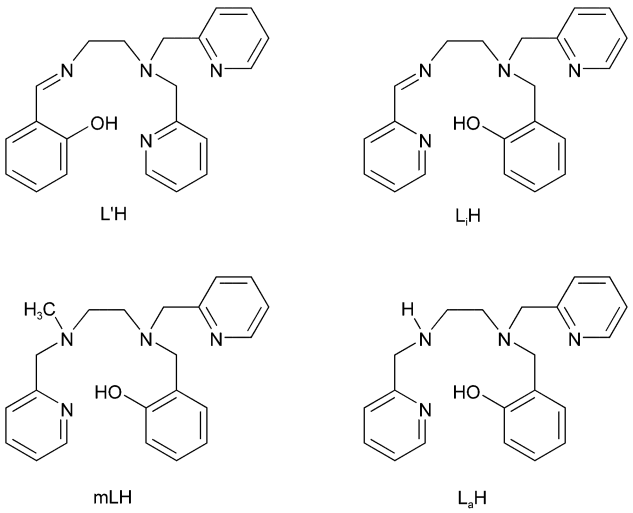

Scheme 1. The mLH ligand used in this work and various other pentadentate ligands for comparison.

We report here the synthesis and the X-ray characterisation of a new phenolato-bridged Mn^{II} dimer [(mL)Mn^{II}-Mn^{II}(mL)](ClO_4)$_2$ (**1**(ClO_4)$_2$). We will demonstrate that the chemical oxidation of **1** with *t*BuOOH leads to the [(mL)Mn^{III}-(μ-O)-Mn^{III}(mL)]$^{2+}$ complex (**2**), which in turn can be electrochemically oxidised into [(mL)Mn^{III}-(μ-O)-Mn^{IV}(mL)]$^{3+}$ (**2ox**). A [Mn^{III}-(μ-O)$_2$-Mn^{IV}]$^{3+}$ core unit system, **3**, can also be generated and we will demonstrate that the EPR signatures of **2ox** and **3** differ significantly. We will also show that the electrochemical oxidation of **1** in the presence of an appropriate base leads to the formation of the desired [(mL)Mn^{III}-(μ-O)-Mn^{IV}(mL)]$^{3+}$ species (**2ox**). Consequently, three oxidative equivalents can be produced from the initial $Mn^{II}Mn^{II}$ complex, with the concomitant formation of a mono-μ-oxo bridge.

Results and Discussion

Attempts to isolate a manganese complex starting from the free ligand and the tris-acetato-Mn^{III} salt were unsuccessful. However, the use of an Mn^{II} salt leads to the formation of the di-μ-phenolato-di-Mn^{II} complex **1**.

Characterisation of [(mL)$Mn^{II}Mn^{II}$(mL)](ClO_4)$_2$ (1(ClO_4)$_2$):

X-ray crystal structure: The structure of the [(mL)Mn^{II}-Mn^{II}(mL)]$^{2+}$ ion (**1**) is very similar to the one of [(L_i)Mn^{II}-Mn^{II}(L_i)]$^{2+}$ described previously.[66] A view of the cation is presented in Figure 1 and selected bond lengths and angles are listed in Table 1. The complex possesses a C_2 axis that

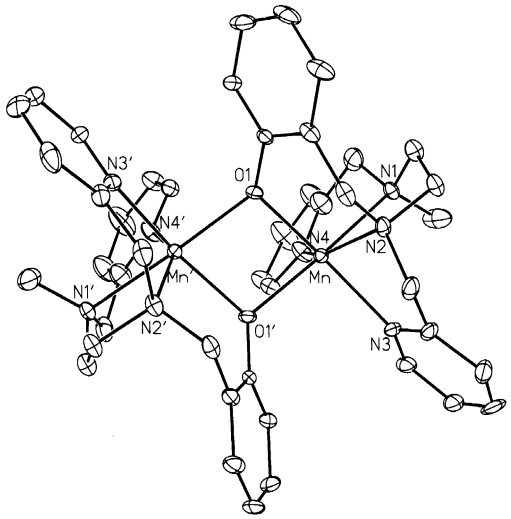

Figure 1. X-ray crystal structure of the cation $[(mL)Mn^{II}Mn^{II}(mL)]^{2+}$.

goes through the middles of the two metallic sites on one hand and of the two phenolic oxygen atoms on the other hand. Each manganese ion is hexacoordinated by the four nitrogen atoms of the mL^- ligand and by two oxygen atoms

Table 1. Selected bond lengths [Å] and angles [°] for **1**.

Mn–O1	2.1225(15)	Mn–N2	2.3079(19)
Mn–O1	2.1351(15)	Mn–N3	2.240(2)
Mn–N1	2.3516(19)	Mn–N4	2.227(2)
O1–Mn–N1	169.10(6)	O1–Mn–N3	155.09(8)
N2–Mn–N4	150.59(7)		
Mn–O1–Mn′	100.01(6)	O1–Mn1–O1′	78.88(6)

originating from the phenolato groups, the first coming from the same ligand and the second from the ligand chelating the other manganese ion. The manganese environment departs from the regular octahedron usually observed for similar hexacoordinated Mn^{II} complexes. The X-ray structure reveals that the folding of the methylated ligand mL^- differs from that of the related ligand L_a^- but is similar to that of L_i^-.[66] This thus confirms the greater flexibility of this kind of ligand when no imine function is present.

The Mn_2O_2 diamond core of the $[(mL)Mn^{II}Mn^{II}(mL)]^{2+}$ cation presents features that are characteristic of the di-μ-phenolato-di-Mn^{II} core unit.[66] The core structure is more regular in **1** than that observed in $[(L_i)Mn^{II}Mn^{II}(L_i)]^{2+}$. The two Mn–O distances differ by less than 0.02 Å, in comparison with a difference of ≈0.03 Å in the previously described complex. The average Mn–O bond length is slighly longer in **1** (2.129 Å versus 2.110 Å), while the bridging Mn–O–Mn angle is very similar (100.0 versus 100.3(2) and 102.5(2)°). However, the Mn···Mn separation is shorter (3.262 versus 3.280 Å) due to a more open O–Mn–O angle (78.9 versus 77.3 and 77.6°). Similar dihedral angles are observed in both systems (11.3 versus 11.5°).

Magnetic susceptibility measurements: The molar magnetic susceptibility, χ_M, of a powder sample of $\mathbf{1}(ClO_4)_2$ was measured in the range 300–2 K. The $\chi_M T$ value as a function of temperature, T, is reported in Figure S1 in the Supporting Information (open circles). At 280 K, the $\chi_M T$ value is 8.04 $cm^3 mol^{-1} K$ and decreases very slowly down to 5.3 $cm^3 mol^{-1} K$ at 20 K. Below 20 K, the $\chi_M T$ value decreases more rapidly, down to 1.14 $cm^3 mol^{-1} K$ at 3 K. This behaviour indicates a weak antiferromagnetic exchange interaction between the two high-spin Mn^{II} ions ($S_1 = S_2 = 5/2$). The best fit is obtained with $g = 1.95$ and $J = -1.8\ cm^{-1}$ ($H = -J\hat{S}_1\hat{S}_2$ (see the Experimental Section) and is also represented in Figure S1 (solid line) in the Supporting Information. These values are in agreement with those reported in the literature for complexes where two Mn^{II} ions are bridged by two phenolates.[67–70] Furthermore, the J value obtained for **1** is very close to that obtained for the 1:1 mixture of the two closely related complexes $[(L_{i/a})Mn^{II}Mn^{II}(L_i)](BPh_4)_2 \cdot H_2O$.[66]

EPR spectroscopy: X-band (9.4 GHz) and Q-band (34 GHz) EPR spectra of a powder sample of $\mathbf{1}(ClO_4)_2$ were recorded over the range 4.2–294 K by using the conventional perpendicular detection mode. The 4.5 K spectra are shown in Figure 2 and the variation upon increasing the temperature

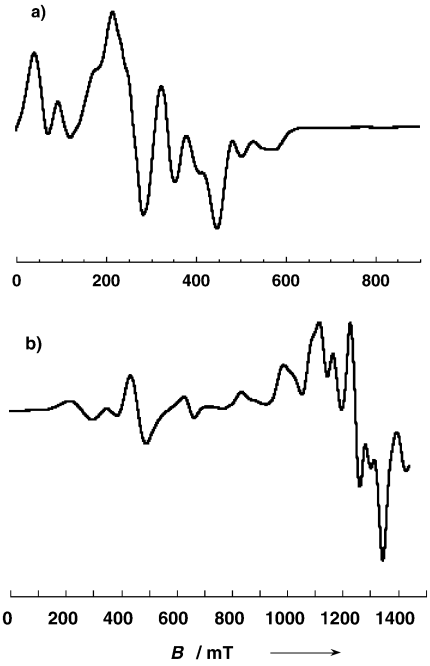

Figure 2. a) X- and b) Q-band EPR spectra recorded on a powder sample of $\mathbf{1}(ClO_4)_2$ at 4.5 K. X-band EPR recording conditions: 9.39 GHz microwave frequency, 0.2 mW microwave power, 0.5 mT modulation amplitude, 100 kHz modulation frequency. Q-band EPR recording conditions: 34 GHz microwave frequency, 0.053 mW microwave power, 0.5 mT modulation amplitude, 100 kHz modulation frequency.

is presented in Figure S2 in the Supporting Information. All spectra exhibit features extending over 0–800 mT at the X band and over 100–1450 mT at the Q band, as usually observed for dinuclear Mn^{II} complexes.[67,71–74] It has long been

demonstrated that these features originate from the superimposition of the signatures of the five paramagnetic S spin states ($S=1$–5).[75] Such mixing makes a detailed analysis of the EPR spectra of dinuclear Mn^{II} systems complicated. Deconvolution procedures have previously been developed that have led, together with the $S=1$ and $S=2$ spin-state traces, to the determination of the exchange coupling constant J between the two antiferromagnetically interacting high-spin Mn^{II} ions.[76–78] More recently, a new methodology has been developed by Blanchard et al. that only relies on a scrupulous examination of the temperature-dependent spectra.[79,80] Up to three individual S-spin-state signatures are determined and it has been shown that the J values obtained are fully consistent with the ones deduced from magnetisation measurements. Whatever the method, the validity of its application relies on a Heisenberg exchange interaction that dominates the other effects contributing to the EPR profiles, such as the Zeeman interaction and the local zero-field splittings. Indeed, a dominant exchange coupling allows the total S spin value to be a good quantum number[81] and allows consideration of the observed EPR spectra as a linear combination of the temperature-independent individual S-spin-state signatures weighted by temperature-dependent coefficients related to the Boltzmann population of the S spin levels. Due to the low value of the exchange coupling constant deduced from the temperature-dependent magnetisation data of **1** ($J=-1.8\,cm^{-1}$), the Zeeman interaction is a competitive effect, at least at 34 GHz. This may lead to inter-S-spin transitions, that are forbidden otherwise.[81] Indeed, the lines observed below 600 mT at the Q band may originate from transitions between the $S=0$ and $S=1$ spin states. A further complication arises from the small energy gaps between the S spin levels at zero field. Even at liquid helium temperatures, the $S=1$–3 spin states are significantly populated and the EPR spectra recorded at 4.2 K are issued from, at least, those three contributions. Increasing the temperature leads to increasing contributions from the $S=4$ and $S=5$ spin states. Above 10 K, no new transitions are detected and further increase of the temperature only leads to changes in the relative line intensities. Therefore, correct analysis of the EPR spectra needs the full diagonalisation of the energy matrix built on the two interacting $S_1=S_2=5/2$ ions, with the Heisenberg (isotropic) exchange interaction, the local Zeeman and zero-field splitting effects and the dipolar coupling all taken into account together with the anisotropic component of the exchange interaction. All these interactions are mathematically reproduced by a tensor that is characterised by three principal values and three principal directions. These tensors are not necessarily colinear and Eular angles are added to set their orientations relative to each other. Hence, the number of unknowns is too important and extra experimental data such as high-field, high-frequency spectra are needed to achieve the EPR analysis. This work is currently in progress.

Compound $\mathbf{1}(ClO_4)_2$ was dissolved in acetonitrile in the presence of 0.1 M tetrabutylammonium perchlorate and EPR spectra were recorded from frozen solutions (see trace a of Figure 6). The spectra recorded at 4.2 K present similar features to those detected for powder samples at both the X and Q bands, a result which proves that the dinuclear structure of complex **1** is maintained in solution. Unfortunately, no Mn-hyperfine structure was observed. This can be attributed to the superimposition, within the same magnetic field range, of several lines originating from the different S spin states and/or from inter-S-spin transitions that exhibit slightly distinct Mn-hyperfine structures.

Chemical oxidation by *t*BuOOH: It was checked that an acetonitrile solution of **1** was stable at room temperature for several days. The chemical oxidation of **1** was performed by the addition of *t*BuOOH to an acetonitrile solution of **1** at room temperature (20 °C). We will show in the following section that the species thus obtained, denoted **2**, is the unsupported mono-μ-oxo complex $[(mL)Mn^{III}\text{-}(\mu\text{-}O)\text{-}Mn^{III}(mL)]^{2+}$. This species spontaneously evolves into the di-μ-oxo species $[Mn^{III}\text{-}(\mu\text{-}O)_2\text{-}Mn^{IV}]^{3+}$ (**3**). When the chemical oxidation of **1** is performed in an electrochemical cell, complex **2** can be electrochemically oxidised into the mixed-valent mono-μ-oxo complex $[(mL)Mn^{III}\text{-}(\mu\text{-}O)\text{-}Mn^{IV}(mL)]^{3+}$ (**2ox**).

*Oxidation of **1** into **2***: The optimum conditions for oxidizing **1** into **2** are reached when 10 equivalents of *t*BuOOH are added to a millimolar acetonitrile solution of $\mathbf{1}(ClO_4)_2$. After a few minutes of stirring under air, the solution changes from colourless to dark purple. The resulting species **2** has been characterised by different techniques. All the data shown below were recorded ten minutes after the addition of *t*BuOOH at 20 °C, since we have determined that the maximum amount of species **2** is available at that time.

The evolution of the X-band EPR spectra recorded upon addition of *t*BuOOH revealed the total disappearance of the signal of **1**. Only a very weak signal is detected at $g=2$ (data not shown); this signal increases with time (see below). Thus, the resulting species **2** is EPR-silent. This suggests the formation of an Mn^{III} complex. Electrospray mass spectra were recorded in positive detection mode (Figure S3 in the Supporting Information). In the starting solution, quasimolecular ions were detected at m/z 931 (monocation, relative intensity 45 %) and 416 (dication, relative intensity 85 %); these correspond to the $\{[(mL)Mn^{II}Mn^{II}(mL)](ClO_4)\}^+$ and the $[(mL)Mn^{II}Mn^{II}(mL)]^{2+}$ ions, respectively. After addition of *t*BuOOH, the peak at m/z 931 significantly decreases while new ones appear at m/z 947 (monocation) and 424 (dication) with relative intensities of 7 and 70 %, respectively. The increases of 16 and 8 units indicate the insertion of one oxygen atom into complex **1** with the concomitant oxidation of both Mn^{II} ions into Mn^{III}. Consequently, these two new peaks may be attributed to the $\{[(mL)Mn^{III}\text{-}(\mu\text{-}O)\text{-}Mn^{III}(mL)](ClO_4)\}^+$ and the $[(mL)Mn^{III}\text{-}(\mu\text{-}O)\text{-}Mn^{III}(mL)]^{2+}$ cations, respectively. Based on the EPR and mass spectroscopy data, we propose that the species formed upon the addition of *t*BuOOH to **1** is the unsupported mono-μ-oxo-di-Mn^{III} complex $[(mL)Mn^{III}\text{-}(\mu\text{-}O)\text{-}Mn^{III}(mL)]^{2+}$ (**2**).

The evolution of the electronic spectrum of **1** upon oxidation with *t*BuOOH is represented in Figure 3a. Before oxi-

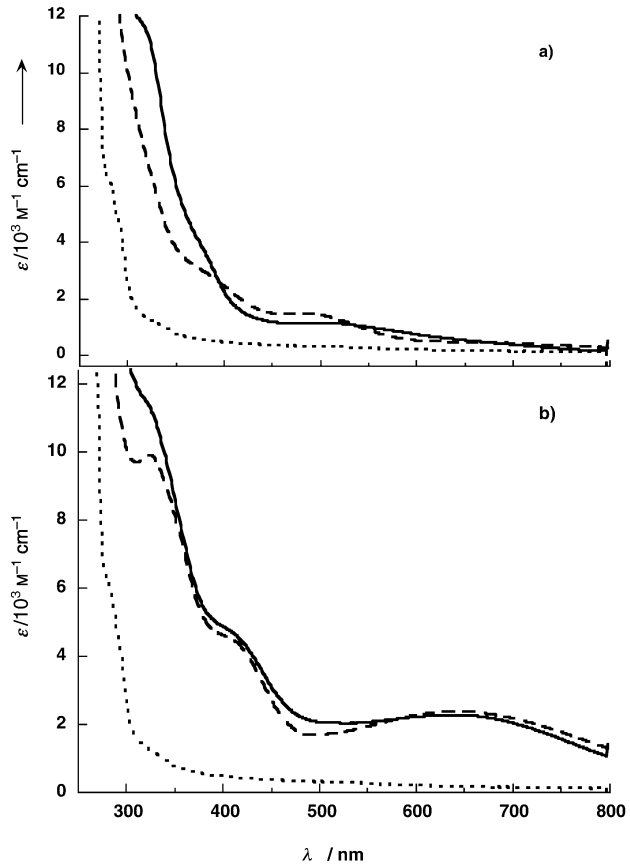

Figure 3. a) Evolution of the UV/Vis spectrum of **1** upon addition of 10 equivalents of *t*BuOOH to 1 mM solution in CH_3CN: before addition (dotted line), after 10 min at room temperature (solid line) and after 1 h at room temperature (dashed line). b) UV/Vis spectrum of **1** before (dotted line) and after (dashed line) complete bulk electrolysis at $E=$ 1.1 V versus the SCE in CH_3CN containing 0.1 M tetrabutylammonium perchlorate, together with the UV/Vis spectrum of **2** (solid line) after electrochemical oxidation at $E=1.1$ V versus the SCE in a thin-layer spectroelectrochemical cell.

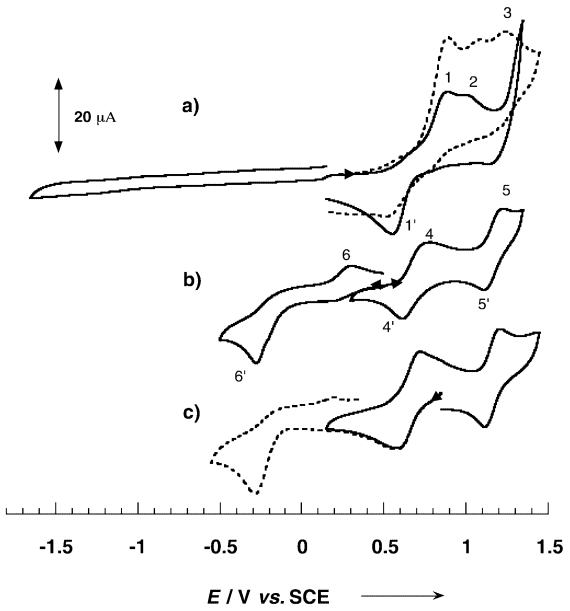

Figure 4. Cyclic voltammograms of 1 mM **1** in acetonitrile in the presence of 0.1 M tetrabutylammonium perchlorate ($T=20$ °C, scan rate = 100 mV s^{-1}): a) with (dashed line) or without (solid line) 1 equivalent of 2,6-lutidine per molecule of **1**; b) 10 min after addition of 10 equivalents of *t*BuOOH; c) after complete bulk electrolysis at $E=1.1$ V versus the SCE in the presence of 1 equivalent of 2,6-lutidine per molecule of **1**.

dation, the spectrum is featureless in the visible region, as expected for a Mn^{II} complex. Only an intense band below 300 nm ($\varepsilon=16\,000$ M^{-1} cm^{-1}) is detected; this band can be attributed to a $\pi\rightarrow\pi^*$ transition within the ligand. After addition of *t*BuOOH, the electronic spectrum exhibits four major absorption bands, located at 507 ($\varepsilon=1020$), 376 ($\varepsilon=$ 3580), 317 ($\varepsilon=10\,160$), and 283 nm ($\varepsilon=15\,520$ M^{-1} cm^{-1}). The absorption band at 507 nm can be attributed to a phenolate$\rightarrow Mn^{III}$ charge-transfer transition. Indeed, a very similar band ($\lambda=506$ nm, $\varepsilon=2100$ M^{-1} cm^{-1}) has been detected by Neves et al.[82] for the $[Mn^{III}(bbpen)]^+$ complex, where the ligands H_2BBPEN[7] and mLH are related by substitution of the methyl group in mLH with a 2-hydroxybenzyl group. In addition, all the features listed above are very similar to those reported for the complex $[(L')Mn^{III}$-(μ-O)-$Mn^{III}(L')]^{2+}$.[34]

The oxidation of **1** was also performed in the electrochemical cell. The recorded cyclic voltammogram (Figure 4b) exhibits two quasireversible anodic waves at $E_4^{1/2}=$ 0.65 V ($\Delta E_p=135$ mV) and $E_5^{1/2}=1.16$ V ($\Delta E_p=100$ mV) and one irreversible cathodic wave at $E_{6'}^{p}=-0.28$ V (all measured versus the standard calomel electrode (SCE)). The $E^{1/2}$ values are reported in Table 2, together with those of other dinuclear Mn–oxo complexes. The 510 mV separation between the two anodic waves (ΔE_{ox}) is far smaller than the ≈800 mV separation generally observed between

Table 2. $E^{1/2}$ potential values of $Mn^{III}Mn^{III}$ dinuclear complexes [V versus SCE].

Ligand	$Mn^{III}Mn^{III}/Mn^{III}Mn^{IV}$	$Mn^{III}Mn^{IV}/Mn^{IV}Mn^{IV}$	Ref.
L'^-	0.54	0.99	[34]
mL^-	0.65	1.16	this work
N,Nbispicen[7]	0.18	0.98	[37]

the $Mn^{III}Mn^{III}/Mn^{III}Mn^{IV}$ and $Mn^{III}Mn^{IV}/Mn^{IV}Mn^{IV}$ oxidation processes in di-μ-oxo-di-Mn complexes.[37,83] Indeed, the shape of the voltammogram is reminiscent of that of $[(L')Mn^{III}$-(μ-O)-$Mn^{III}(L')]^{2+}$, for which $\Delta E_{ox}=450$ mV.[34] This supports the formation of $[(mL)Mn^{III}$-(μ-O)-$Mn^{III}(mL)]^{2+}$ upon addition of *t*BuOOH to **1**. Therefore, the oxidation waves observed at $E_4^{1/2}=0.65$ V and $E_5^{1/2}=1.16$ V versus the SCE are attributed to the oxidation of $[(mL)Mn^{III}$-(μ-O)-$Mn^{III}(mL)]^{2+}$ (**2**) into $[(mL)Mn^{III}$-(μ-O)-$Mn^{IV}(mL)]^{3+}$ (**2ox**) and of $[(mL)Mn^{III}$-(μ-O)-$Mn^{IV}(mL)]^{3+}$ into $[(mL)Mn^{IV}$-(μ-O)-$Mn^{IV}(mL)]^{3+}$, respectively. The irreversible cathodic wave at $E_{6'}^{p}=-0.28$ V versus the SCE corresponds to the reduction of $[(mL)Mn^{III}$-(μ-O)-$Mn^{III}(mL)]^{3+}$ (**2**) into $[(mL)Mn^{II}$-(μ-O)-$Mn^{III}(mL)]^{2+}$, which is not stable under the experimental conditions. We propose that at this oxidation state the dimeric structure breaks down to form monomeric complexes, as suggested by the presence of the wave at $E_6^{p}=0.29$ V versus the SCE on the reverse scan.

*Evolution of **2** into **3***: As indicated by the evolution of the EPR spectrum, species **2** is not stable at room temperature. The very weak signal detected at $g=2$ after the addition of *t*BuOOH to **1** (see above) increases with time and reaches a maximum after approximately 10 h. This spectrum presents 16 lines spread over 124.5 mT with a regular spacing of 7.5 mT (Figure 5b). This signal is characteristic of a mixed-valent $[Mn^{III}\text{-}(\mu\text{-}O)_2\text{-}Mn^{IV}]^{3+}$ core complex. A simulation has been performed by using the commonly used hypothesis for such systems (see the Experimental Section). The parameters used for the simulation are listed in Table 3. The $\tilde{g}$ tensor presents a very small anisotropy ($g_x-g_z=0.02$). This value is fully consistent with those determined for di-μ-oxo and di-μ-oxo-μ-acetato $Mn^{III}Mn^{IV}$ complexes by using high-field, high-frequency EPR spectroscopy,[36,60–62] which is a more reliable technique as far as the g anisotropy is concerned. The $\tilde{A}_1$ hyperfine tensor is found to be of rhombic symmetry while the $\tilde{A}_2$ hyperfine tensor is almost isotropic. In addition, the isotropic components of both tensors are in a 2:1 ratio and are close to the values reported in the literature for $[Mn^{III}\text{-}(\mu\text{-}O)_2\text{-}Mn^{IV}]^{3+}$ complexes.[28,36,37,60,61] Therefore, the subscripts 1 and 2 used in the description of the simulation are assigned to the Mn^{III} and Mn^{IV} sites, respectively. We, thus, propose that complex **2** spontaneously evolves into $[(mL)Mn^{III}\text{-}(\mu\text{-}O)_2\text{-}Mn^{IV}(mL)]^{n+}$, denoted **3**, in which one of the aromatic groups of the ligand would be uncoordinated. The tetracoordination of a potentially pentadentate ligand has already been observed in $[(mL_5)ClFe^{III}\text{-}(\mu\text{-}O)\text{-}Fe^{III}Cl(mL_5)]^{2+}$.[7,84] The quasi-ideal superimposition of the recorded X-band EPR spectrum with that of $[(mL_4)Mn^{III}\text{-}(\mu\text{-}O)_2\text{-}Mn^{IV}(mL_4)]^{3+}$[7] suggests that the pendent arm is the phenol ring, which in addition would be protonated, thereby leading to an overall 3+ charge for complex **3**. In fact, the definite identification of the uncoordinated arm of the ligand would require isolation of **3**, since the conversion of **2ox** into **3** is not complete. Indeed, quantification measurements made on the EPR spectrum of a solution of **2** after 10 h indicate that species **3** only accounts for 15% of the total. Fortunately, the other species are EPR-silent (Mn^{III} or strongly antiferromagnetically coupled di-Mn^{IV} species) and allow the detection of **3** by EPR spectroscopy.

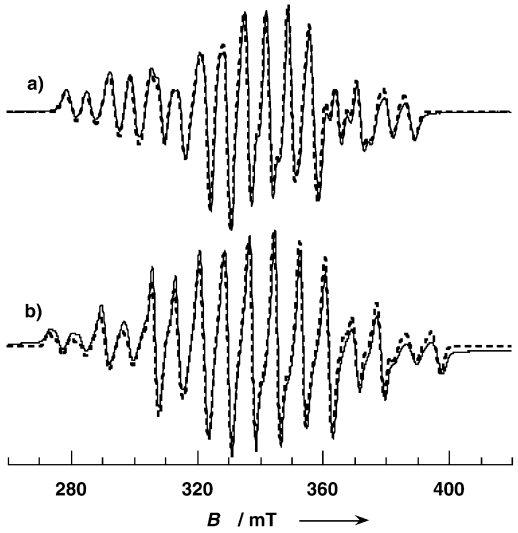

Figure 5. Experimental (solid line) and simulated (dashed line) X-band EPR spectra recorded on acetonitrile solutions containing 0.1 M tetrabutylammonium perchlorate: a) $[(mL)Mn^{III}\text{-}(\mu\text{-}O)\text{-}Mn^{IV}(mL)]^{3+}$ (**2ox**); b) $[(mL)Mn^{III}\text{-}(\mu\text{-}O)_2\text{-}Mn^{IV}(mL)]^{n+}$ (**3**). Recording conditions: 0.5 mT modulation amplitude, 100 kHz modulation frequency, $T=100$ K, 2 mW microwave power, $\nu=$ a) 9.420, b) 9.386 GHz microwave frequency. Simulation parameters: half-width at half-height = 1.15 mT (a), 1.25 mT (b); agreement factor $R=0.030$ (a), 0.016 (b).

Table 3. EPR parameters determined by simulation performed with rhombic but colinear tensors. Hyperfine coupling constants are given in cm^{-1}.

		g	$\lvert A_1\rvert$	$\lvert A_2\rvert$	Ref.
$[(L')Mn^{III}\text{-}(\mu\text{-}O)\text{-}Mn^{IV}(L')]^{3+}$	x	2.006	0.0160	0.0062	[34]
	y	1.997	0.0130	0.0059	
	z	1.982	0.0091	0.0062	
	iso	1.995	0.0127	0.0061	
2ox	x	2.005	0.0146	0.0062	
	y	2.003	0.0139	0.0060	this
	z	1.985	0.0089	0.0065	work
	iso	1.997	0.0124	0.0062	
3	x	2.001	0.0164	0.0069	
	y	1.996	0.0149	0.0076	this
	z	1.984	0.0114	0.0072	work
	iso	1.994	0.0142	0.0072	

*Electrochemical oxidation of **2** into **2ox***: The generation of the expected mixed-valent, unsupported, mono-μ-oxo complex $[(mL)Mn^{III}\text{-}(\mu\text{-}O)\text{-}Mn^{IV}(mL)]^{3+}$ (**2ox**) can be predicted from the one-electron oxidation of species **2**. Indeed cyclic voltametry, EPR, and UV/Vis data recorded on an electrolysed solution of **2** at $E=1.1$ V versus the SCE demonstrate the formation of **2ox**.

The oxidation of **1** was performed in the electrochemical cell. Ten minutes after the addition of *t*BuOOH had been completed, the temperature was decreased to −30 °C in order to slow down the spontaneous evolution of **2** (see above). A cyclic voltamogram was recorded on the electrolysed solution after the comsumption of one electron per molecule of **2** (not shown). Starting from $E=1.1$ V versus the SCE, the trace displays one reversible wave when scanning towards negative potentials ($E^{1/2}=0.65$ V versus the SCE) and one reversible wave when scanning towards positive potentials ($E^{1/2}=1.16$ V versus the SCE). These data are fully consistent with the reduction of $[(mL)Mn^{III}\text{-}(\mu\text{-}O)\text{-}Mn^{IV}(mL)]^{3+}$ (**2ox**) into $[(mL)Mn^{III}\text{-}(\mu\text{-}O)\text{-}Mn^{III}(mL)]^{2+}$ (**2**) and the oxidation of $[(mL)Mn^{III}\text{-}(\mu\text{-}O)\text{-}Mn^{IV}(mL)]^{3+}$ (**2ox**) into $[(mL)Mn^{IV}\text{-}(\mu\text{-}O)\text{-}Mn^{IV}(mL)]^{4+}$, respectively.

EPR spectra were recorded at $T=4.2$ K on 100-μL aliquots that were taken regularly (every 100 mC) during the bulk electrolysis of **2**. The series of spectra exhibit a multiline signal centred at $g=2$ that increases in intensity as the electrolysis progresses. A scrupulous examination of this signal reveals the superimposition of two $Mn^{III}Mn^{IV}$–oxo signatures. Actually, the central lines increase remarkably in intensity while the two outmost features remain constant during the course of the electrolysis. Moreover, the lowest and highest field lines exactly coincide in position with

those observed for the EPR signature of the di-μ-oxo-di-Mn complex **3**. We thus suggest that a new $Mn^{III}Mn^{IV}$ species arises in addition to the small amount of **3** resulting from the spontaneous evolution of **2**.

Two different procedures were performed in order to deconvolute the recorded signal. In a first approach, the EPR signal associated with **3** was substracted from the recorded spectra after scaling of the two outmost lines. The second method involved subtracting two successive spectra. Both strategies led to the same signal that spread 16 lines over the range 278–389 mT (first peak to last trough). This spectral width of 111 mT is significantly smaller than the width of 125 mT typically observed for $[Mn^{III}\text{-}(\mu\text{-}O)_2\text{-}Mn^{IV}]^{3+}$ core complexes. Indeed, this is reminiscent of the spectral width value (119 mT) reported for $[(L')Mn^{III}\text{-}(\mu\text{-}O)\text{-}Mn^{IV}(L')]^{3+}$.[34] This result strongly suggests that electrochemical oxidation of **2** leads to the formation of $[(mL)Mn^{III}\text{-}(\mu\text{-}O)\text{-}Mn^{IV}(mL)]^{3+}$ (**2ox**). No simulation was attempted on this deconvoluted signal. As will be described in the next section, a genuine EPR signal (with no contaminating **3** species) was recorded on a solution of pure **2ox** generated by direct electrolysis of **1** in the presence of base.

The oxidation of **2** into **2ox** was also characterised by in situ spectroelectrochemistry. The UV/Vis spectrum (Figure 3b) recorded after the initial solution of **2** has been electrolysed ($E = 1.1$ V versus the SCE) presents three well-defined absorption bands at 643 ($\varepsilon = 2300$), 414 ($\varepsilon = 4500$) and 325 nm ($\varepsilon = 11\,200\ M^{-1}\,cm^{-1}$). Such characteristics are similar to those previously observed for the $[(L')Mn^{III}\text{-}(\mu\text{-}O)\text{-}Mn^{IV}(L')]^{3+}$.[34] The broad absorption band at 643 nm can be attributed to the phenolate→Mn^{IV} charge-transfer transition, as reported in the literature.[82,85,86] The two other bands are consistent with oxo→Mn^{IV} charge-transfer transitions, as described for the $[Mn_2(\mu\text{-}O)_2]$ core.[37,64,87,88]

We shall also report that a solution of **2ox** could equally be obtained by addition of one equivalent of protons to a freshly prepared solution of **2**. This has been fully established by the same techniques. Dismutation of di-Mn^{III} complexes generating mixed-valent $Mn^{III}Mn^{IV}$ species is known to be favoured in the presence of protons.[65]

Electrochemical oxidation: In the following section, we will demonstrate that **2ox** can be prepared by direct electrolysis of **1**.

Cyclovoltammetry of ***1****(ClO$_4$)$_2$*: The cyclic voltammogram of 1 mM **1** in acetonitrile in the presence of 0.1 M tetrabutylammonium perchlorate is shown in Figure 4a. The cyclic voltammetry trace of **1** presents two successive anodic waves (labelled 1 and 2) at $E_1^p = 0.89$ V and $E_2^p = 1.02$ V, accompanied on the reverse scan by an ill-defined cathodic wave (labelled 1′) at $E_{1'}^p = 0.56$ V (all measured versus the SCE). The anodic process is attributed to the two-step oxidation of $[(mL)Mn^{II}Mn^{II}(mL)]^{2+}$ into $[(mL)Mn^{III}Mn^{III}(mL)]^{4+}$. The potential values are slightly higher than the ones reported for the related 1:1 mixture of $[(L_{i/a})Mn^{II}Mn^{II}(L_i)](ClO_4)_2\cdot H_2O$.[66] This can be attributed firstly to greater steric hindrance due to the methyl substituent.[89,90] However, these potentials are fairly high compared to the reported literature values. Mn^{II}/Mn^{III} oxidation potentials have been reported at 0.6 V versus the SCE with monodentate phenolato ligands.[91,92] In the present case, the observed higher value could originate from a bridging coordination mode of the phenolate moieties that will not stabilise high oxidation states of the Mn ions. From a structural point of view, the studied complex can easily evolve upon oxidation into two similar mononuclear Mn complexes where the phenolato group is monodentate. Actually, when increasing the scan rate or decreasing the temperature, the value of the ratio of the peak intensities $I_p^1:I_p^2$ decreases (data not shown). This effect can be interpreted by considering a competition between an electrochemical–electrochemical process and an electrochemical–chemical mechanism. Indeed, after the $[(mL)Mn^{II}Mn^{III}(mL)]^{3+}$ species has been formed, it can be further oxidised into $[(mL)Mn^{III}Mn^{III}(mL)]^{4+}$ or it can evolve chemically. Good candidates for the products of this chemical evolution are Mn^{II} and Mn^{III} monomeric species such as $[(mL)Mn^{II/III}(S)]^{n+}$ where S is either a solvent or a water molecule. When the scan rate is high enough or the temperature low enough, the chemical evolution is frozen and the intermediate mixed-valence $[(mL)Mn^{II}Mn^{III}(mL)]^{3+}$ compound can be further oxidised. This two-step oxidation is irreversible, as demonstrated by the lack of the associated reduction wave, which means that the $[(mL)Mn^{III}\text{-}Mn^{III}(mL)]^{4+}$ compound is not stable and ultimately evolves into $[(mL)Mn^{III}(S)]^{2+}$. On the reverse scan, the cathodic process (1′) can then be interpreted as the reduction of this species. Indeed, Mn^{II}/Mn^{III} redox processes involving doubly charged Mn^{III} ions have been reported in the literature at around 0.5 V versus the SCE.[91]

Bulk electrolytic oxidation of ***1*** *into* ***2ox*** *in the presence of base*: Figure 4a shows the evolution of the cyclic voltammetry of a solution of **1** upon addition of one equivalent per manganese ion of 2,6-dimethylpyridine (also named 2,6-lutidine). A new peak appears at $E_3^p = 1.24$ V versus the SCE. It was confirmed that this new peak is not due to the added lutidine. It is attributed to the oxidation of an $[(mL)Mn^{III}(OH)]^{+}$ species resulting from the deprotonation of the coordinated water molecule in $[(mL)Mn^{III}(OH_2)]^{2+}$. This mononuclear Mn^{III} species originates from the breaking of the dinuclear structure of **1** when reaching the $Mn^{II}Mn^{III}$ or the $Mn^{III}Mn^{III}$ oxidation state.[93]

A solution of **1** containing 1 equivalent of 2,6-lutidine per manganese ion was oxidised by controlled-potential electrolysis at $E = 1.1$ V versus the SCE. The solution changed from colourless to dark purple before turning dark blue. After 1.5 oxidizing equivalents per manganese ion, the current intensity faded. Cyclic voltametry of the resulting solution exhibits one well-defined reversible ($\Delta E^{1/2} = 100$ mV) oxidation wave at $E^{1/2} = 1.16$ V, one well-defined reversible ($\Delta E^{1/2} = 135$ mV) reduction wave at $E^{1/2} = 0.65$ V and one irreversible reduction wave at $E^p = -0.28$ V (all measured versus the SCE; Figure 4c). Comparison between traces b and c of Figure 4 strongly suggests that the product of the bulk electrolysis of **1** is identical to compound **2ox**. This is also supported by UV/Vis and EPR spectra recorded during the course of the bulk electrolysis.

The absorption spectrum recorded after the complete electrolytic oxidation (Figure 3b) presents a drastic difference in the 400–800 nm range in comparison to the featureless initial spectrum.[94] This spectrum presents two absorption bands at 650 ($\varepsilon = 2300$) and 412 nm ($\varepsilon = 4430\ cm^{-1}\,M^{-1}$). Furthermore, this trace almost superimposes in the visible region with that of **2ox** (Figure 3b) except for a slightly lower absorption value around 490 nm. This lower value is a good indication that the present solution is not contaminated by other compounds as opposed to what was observed when **2ox** was generated by the electrochemical oxidation of **2**.

During the electrolysis, 100-μL aliquots of the solution were taken and the EPR spectra were collected. The evolution of the X-band EPR signal is reported in Figure 6.

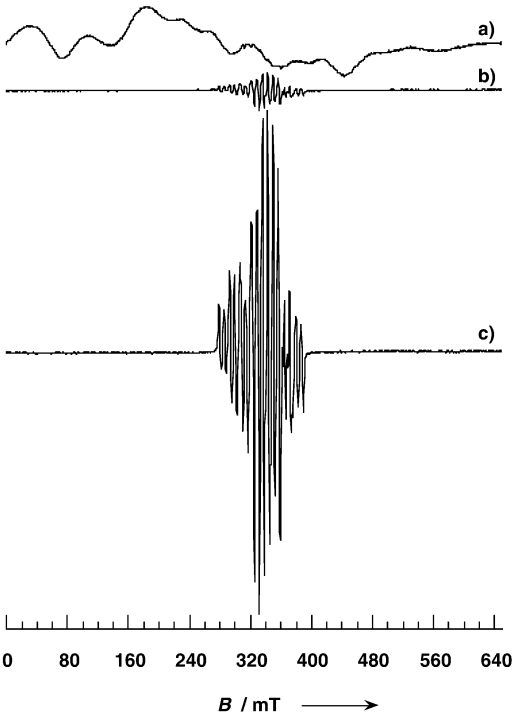

Figure 6. Evolution of the X-band EPR spectrum of **1** during bulk electrolysis at $E = 1.1$ V versus the SCE in acetonitrile containing 0.1 M tetrabutylammonium perchlorate: a) before electrolysis; b) after 2.3 electrons per molecule of **1**; c) after 3 electrons per molecule of **1**. Recording conditions: 0.5 mT modulation amplitude, 100 kHz modulation frequency, $T = 10$ K, 0.008 mW microwave power, $\nu =$ a) 9.38, b) 9.383 and c) 9.38 GHz microwave frequency.

Trace a was recorded before the electrolysis started and corresponds to the signature of species **1**, as described above. After consumption of 2.3 electrons per molecule of **1** (Figure 6b), the signal of **1** disappears and a very weak multiline signal centred at $g = 2$ appears. After consumption of 3 electrons per molecule of **1**, this signal has gained in intensity and exhibits 16 lines that are regularly separated by approximately 7 mT; this signal is characteristic of a mixed-valent $Mn^{III}Mn^{IV}$ dinuclear complex (Figure 6c). The spectral width of 111 mT (first peak to last trough) is identical to that of the X-band EPR signal reported above for compound **2ox**. The similarities of the EPR signatures of the present electrolysed solution and of a solution of **2ox** (resulting from the electrolysis of **2** as described above) strongly suggest that the two compounds are identical. We thus propose that the electrolysis of **1** at the working potential of 1.1 V versus the SCE leads to the formation of $[(mL)Mn^{III}$-$(\mu\text{-}O)$-$Mn^{IV}(mL)]^{3+}$ (**2ox**).

The EPR spectrum was simulated according to the commonly used theoretical frame for mixed-valent $Mn^{III}Mn^{IV}$ systems (Figure 5a). The results are reported in Table 3. The $\tilde{g}$ tensor presents a very weak anisotropy with an isotropic component slighlty lower than 2. This is fairly consistent with an $S = 1/2$ system. The $\tilde{A}_1$-hyperfine tensor is found to be close to axial symmetry while the $\tilde{A}_2$-hyperfine tensor is almost isotropic. In addition, the isotropic components of both tensors are in a 2:1 ratio. These features are characteristic of an $Mn^{III}Mn^{IV}$ system, with the subscripts 1 and 2 corresponding to the Mn^{III} and Mn^{IV} sites, respectively. The Mn-hyperfine isotropic values determined for the **2ox** species (124×10^{-4} and $62\times10^{-4}\ cm^{-1}$) are significantly smaller than the ones reported for $[Mn^{III}$-$(\mu\text{-}O)_2$-$Mn^{IV}]^{3+}$ core units (averaged values are 140×10^{-4} and $70\times10^{-4}\ cm^{-1}$) and close to those determined for $[(L')Mn^{III}$-$(\mu\text{-}O)$-$Mn^{IV}(L')]^{3+}$ (127×10^{-4} and $61\times10^{-4}\ cm^{-1}$). A detailed examination of the Mn^{III}-hyperfine tensor principal values reveals differences between **2ox** and $[(L')Mn^{III}$-$(\mu\text{-}O)$-$Mn^{IV}(L')]^{3+}$. Firstly, the x component is significantly smaller in **2ox** (146×10^{-4} versus $160\times10^{-4}\ cm^{-1}$). This is the origin of the smaller X-band spectral width detected experimentally for **2ox** relative to that of $[(L')Mn^{III}$-$(\mu\text{-}O)$-$Mn^{IV}(L')]^{3+}$. Secondly, the rhombicities differ: the $(|A_{1x}|-|A_{1y}|)/(|A_{1y}|-|A_{1z}|)$ ratios for **2ox** and $[(L')Mn^{III}$-$(\mu\text{-}O)$-$Mn^{IV}(L')]^{3+}$ are equal to 0.14 and 0.77, respectively. This may originate from the differences in the pentacoordinated ligands. In $[(L')Mn^{III}$-$(\mu\text{-}O)$-$Mn^{IV}(L')]^{3+}$, the nitrogen imine atom is in the *trans* position relative to the bridging oxo atom and the two pyridine rings are *trans* to each other, thereby defining the Jahn–Teller elongation axis of the Mn^{III} site. On the other hand, if one assumes that the coordination of the manganese ions is unchanged in **2ox** relative to the coordination in **1**, with the Mn–O1′ and Mn′–O1 bonds in **1** being replaced by the Mn–(μ-O) links, the two pyridine rings would be *cis* to each other and the nitrogen amine atom, N1 or N1′, would be *trans* to the bridging oxo atom. Such differences in the coordination sphere may lead to a different Jahn–Teller distortion around the Mn^{III} centre and thus to differences in the electronic effects that are reflected in the principal values of the Mn^{III}-hyperfine tensor.

Formation of the μ-oxo bridges: Starting from the di-μ-phenolato-di-Mn^{II} complex **1**, we have shown that the unsupported mono-μ-oxo-di-manganese core unit can be formed upon chemical or electrochemical oxidation. Although it would be surprising if both oxidations proceeded according to the same mechanism, the present study affords a unique opportunity to propose intermediates on the route from the Mn^{II} to Mn–oxo clusters.

Electrochemical interconversion of mononuclear Mn^{II} into dinuclear $Mn^{III}Mn^{IV}$ complexes with the concomitant

formation of oxo bridges has been previously reported in the literature. In these cases, one of the exogenous ligands (namely acetate) or the ligand itself served as an internal base for the deprotonation of the water molecules.[55,95,96] Since the ligand:Mn ratio is 1 in the starting material **1** as in the resulting complex **2ox**, we have chosen to add an external base to assist the formation of the oxo bridge. The choice of 2,6-lutidine was guided by the will to use a non-coordinating base with a high oxidation potential.

A complete mechanism leading to the formation of **2ox** is proposed in Scheme 2 where B stands for 2,6-lutidine. In the

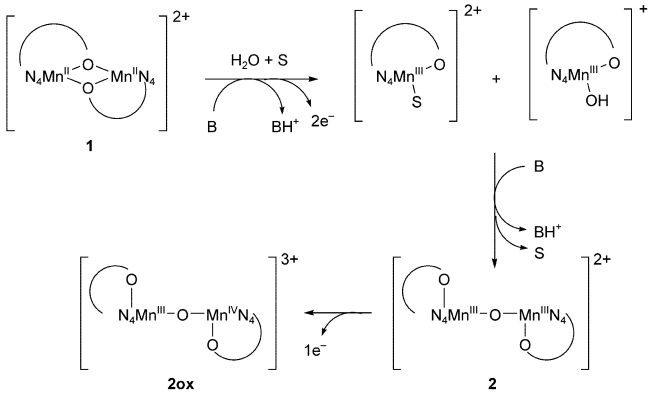

Scheme 2. Proposed mechanism for the electrochemical formation of **2ox**.

present scheme, the water molecule comes from residual water in the acetonitrile solvent. The initial step is the oxidation of the $Mn^{II}Mn^{II}$ dimer **1** that leads to the breaking of the phenolato bridges and the generation of monomeric Mn^{III} complexes. A key species is $[(mL)Mn^{III}(OH)]^+$ which originates from the deprotonation of the aquo complex $[(mL)Mn^{III}(OH_2)]^+$. The condensation of two mononuclear Mn^{III} species, one of which being $[(mL)Mn^{III}(OH)]^+$, leads to the dinuclear Mn^{III} complex **2**. This step requires one additional equivalent of base per molecule of **1**. Thus, a total of two equivalents of base per molecule of **1** is needed to form the oxo bridge. At this point, the applied electrolysis potential is high enough ($E = 1.1$ V versus the SCE) to oxidise further the EPR-silent $[(mL)Mn^{III}\text{-}(\mu\text{-}O)\text{-}Mn^{III}(mL)]^{2+}$ dinuclear species **2** into the mixed-valent EPR-active $[(mL)Mn^{III}\text{-}(\mu\text{-}O)\text{-}Mn^{IV}(mL)]^{3+}$ complex **2ox**. The overall electrochemical process is summarised in Equation 1.

$$[(mL)Mn^{II}Mn^{II}(mL)]^{2+} + H_2O + 2\,B \rightarrow [(mL)Mn^{III}\text{-}(\mu\text{-}O)\text{-}Mn^{IV}(mL)]^{3+} + 2\,BH^+ + 3\,e^- \quad (1)$$

It is worth noticing that several experimental arguments support the proposed mechanism. Firstly, an EPR-silent step is indeed observed during the course of the electrolysis before the growth of the 111 mT width EPR signal that is characteristic of the $[(mL)Mn^{III}\text{-}(\mu\text{-}O)\text{-}Mn^{IV}(mL)]^{3+}$ species **2ox**. Secondly, a transient reddish colour is observed as the electrolysed solution changes from colourless (complex **1**) to dark blue (complex **2ox**). Even though this reddish colouration cannot unambigously be attributed to a specific Mn^{III} system, it is likely that it corresponds to some EPR-silent species. Thirdly, the unsupported mono-μ-oxo bridge system exists in the $Mn^{III}Mn^{III}$ oxidation state as described above and is thus a meaningful precursor of the ultimate observed species **2ox**. In addition, the oxidation potential of the $[Mn^{III}\text{-}(\mu\text{-}O)\text{-}Mn^{III}]^{4+}$ core complex **2** is 0.65 V versus the SCE, which leads to the conversion of **2** into **2ox** at the working potential of 1.1 V versus the SCE. It is worth noticing that the one-electron reduction wave of **2ox** present on the cyclic voltammogram recorded at the end of the electrolysis of **1** (Figure 4c) is reversible. This means that, in the presence of the protonated 2,6-lutidine, the $[Mn^{III}\text{-}(\mu\text{-}O)\text{-}Mn^{III}]^{4+}$ core unit remains unprotonated.

In order to tackle the role of the base, bulk electrolyses have been performed with different amounts of 2,6-lutidine. Preliminary results indicate that when no base or only one equivalent of 2,6-lutidine per molecule of **1** is present, the electrolysed solution remains EPR-silent. Furthermore, UV/Vis signatures support the presence of Mn^{III} species and the recording of slightly different absorption spectra depending on the amount of base introduced suggests distinct chemical compositions for the oxidised solutions. This work is under progress.

We have shown that the di-μ-oxo-di-Mn complex is also accessible in the mixed-valent $Mn^{III}Mn^{IV}$ state (complex **3**). Consequently, the formation of a second oxo bridge from the electrochemical oxidation of **1** has been considered by addition of two extra equivalents of 2,6-lutidine per molecule of **1**. When the electrolysis is pursued in the presence of four equivalents of base per molecule of **1**, no condensation of a second water molecule to generate a di-μ-oxo-di-Mn core complex has been observed. For instance, the UV/Vis spectrum recorded when the electrolysis is completed is identical to that of **2ox**. This suggests that water molecules or hydroxy moieties are not able to substitute one of the aromatic arms of the ligand mL^-.

According to the proposed mechanism, complex **2** is an intermediate in the electrochemical oxidation of **1** into **2ox**, but it can hardly be isolated. When the oxidation of **1** is performed with *t*BuOOH, **2** has been clearly identified. One can propose that the insertion of the oxo group involves a high oxidation state of the Mn ion, such as an Mn^{IV}=O species, as depicted in Scheme 3. The overall reaction is given in Equation 2.

$$[(mL)Mn^{II}Mn^{II}(mL)]^{2+} + t\text{BuOOH} \rightarrow [(mL)Mn^{III}\text{-}(\mu\text{-}O)\text{-}Mn^{III}(mL)]^{2+} + t\text{BuO}^- + H^+ \quad (2)$$

The first step in the proposed mechanism would be the addition of one peroxide molecule onto one of the Mn^{II} ions of the dinuclear complex **1**. The heterolytic breaking of the O–O bond would generate a monomeric Mn^{IV}–oxo species, concomitantly with the release of *tert*-butylhydroxide. The condensation of this high-valent Mn–oxo complex with the other Mn^{II} moiety of the initial complex **1** leads to the formation of the oxo bridge with the concomitant oxidation of the Mn^{II} site by the Mn^{IV} ion to result in the experimentally

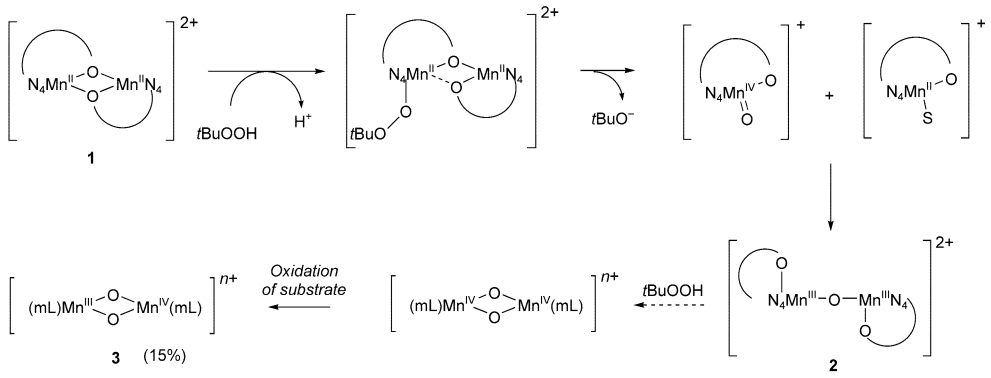

Scheme 3. Proposed mechanism for the chemical formation of **2** and its evolution to **3**.

observed $[(mL)Mn^{III}\text{-}(\mu\text{-}O)\text{-}Mn^{III}(mL)]^{2+}$ complex (**2**). A similar mechanism has already been proposed in the literature for the alkene epoxidation catalysed by Mn–salen complexes[97] and has recently been proved by mass spectrometric measurements.[98,99] In these reported cases, the initial Mn complexes are in the +III oxidation state and thus the detected intermediate species is a Mn^{V}=O complex. Such a mechanism is also invoked by Larson and Pecoraro for the formation of di-μ-oxo-di-Mn^{IV} complexes from $Mn^{III}Mn^{III}$ systems with *t*BuOOH as the oxidant.[100] Based on the present experimental results and in the absence of low-temperature experiments, the proposed Mn^{IV}=O species is only putative. Moreover, the bridging oxygen atom could also come from a water molecule, since a terminal oxo moiety is subject to water molecule exchange.

Under the present experimental conditions, complex **2** ultimately evolves into a mixture of dinuclear $[(mL)Mn^{III}\text{-}(\mu\text{-}O)_2\text{-}Mn^{IV}(mL)]^{n+}$ (**3**) and other EPR-silent species. We propose that the formation of the second oxo bridge results from the reaction of *t*BuOOH with the already present $[(mL)Mn^{III}\text{-}(\mu\text{-}O)\text{-}Mn^{III}(mL)]^{2+}$ complex, to generate an $[Mn^{IV}\text{-}(\mu\text{-}O)_2\text{-}Mn^{IV}]^{4+}$ core species. This second insertion would be slower than the first one since it requires the displacement of one of the aromatic arms. The possible breaking of one of the aromatic arms cannot be totally excluded in the presence of a strong oxidant. The generated Mn^{IV}-Mn^{IV} species would then oxidise either a solvent molecule or the ligand itself to result in the EPR-active $[Mn^{III}\text{-}(\mu\text{-}O)_2\text{-}Mn^{IV}]^{3+}$ core complex **3**.

Conclusion

A new $Mn^{II}Mn^{II}$ dinuclear complex has been obtained with a pentadentate ligand offering an $[N_4O]$ coordination sphere. We have shown that chemical oxidation of this phenolato-bridged $Mn^{II}Mn^{II}$ species (**1**) by *t*BuOOH leads to the formation of the unsupported mono-μ-oxo-bridged complex $[(mL)Mn^{III}\text{-}(\mu\text{-}O)\text{-}Mn^{III}(mL)]^{2+}$ (**2**). In the presence of an excess of *t*BuOOH, complex **2** ultimately evolves into the mixed-valent di-μ-oxo $[Mn^{III}\text{-}(\mu\text{-}O)_2\text{-}Mn^{IV}]^{3+}$ core complex (**3**). Complex **2** can also be electrochemically oxidised into the unsupported mono-μ-oxo-bridged mixed-valent complex $[(mL)Mn^{III}\text{-}(\mu\text{-}O)\text{-}Mn^{IV}(mL)]^{3+}$ (**2ox**). Another route to prepare a pure sample of **2ox** is the direct electrochemical oxidation of **1** in presence of an external base. With the same ligand, we have thus obtained three types of bridges, with the Mn ions in different oxidation states.

The distinction between the mono-μ-oxo and the di-μ-oxo complexes was made possible thanks to a thorough analysis of the EPR signals of the two species. Indeed the simulated parameters for the two $Mn^{III}Mn^{IV}$ mixed-valent complexes showed Mn-hyperfine isotropic values significantly smaller for the mono-μ-oxo system (**2ox**) than for the di-μ-oxo system (**3**). This has already been reported for another mono-μ-oxo Mn^{III}–O–Mn^{IV} complex.[34]

No structural data are available so far for complexes **2** and **2ox**. Linear Mn–O–Mn units have been reported for $[(L')Mn^{III}\text{-}(\mu\text{-}O)\text{-}Mn^{III/IV}(L')]^{2+/3+}$[34] but a bent structure has been observed in $[(m_1L_4)(Cl)Fe^{III}\text{-}(\mu\text{-}O)\text{-}Fe^{III}(Cl)(m_1L_4)]^{2+}$.[7,84] If the two pyridine rings of mL^- in the μ-oxo species are in the *cis* position relative to each other, as they are in **1**, it is unlikely that the core units of complexes **2** and **2ox** are linear. Resonance Raman studies would be of great help in settling this point.

A mechanism involving the condensation of two Mn^{III} moieties is proposed for the direct electrochemical preparation of **2ox**. The oxo bridge is formed by the deprotonation of a water molecule, thanks to the presence of an external base in the solution. This is, to our knowledge, the first time that an extra base has been added to the medium to assist the formation of oxo bridges. Based on this electrochemical method, the preparation of a number of other Mn–oxo clusters can be anticipated. Work in this direction is under progress with polypyridyl ligands.

A putative Mn^{IV}=O intermediate is proposed in the mechanism of chemical formation of the oxo bridge of complex **2**. Even though no experimental data are available so far, it is likely that in this case the oxo bridge is the result of the insertion of an oxo moiety rather than of a condensation process. Low-temperature experiments as well as stopped-flow spectroscopy measurements would undoubtedly help in the assessment of the mechanism. In particular, the recording and analysis of a pure Mn^{IV}=O EPR signal remains a challenging task. It is anticipated that working with bulkier ligands will prevent the condensation step and thus favour the detection of mononuclear intermediates. Several Mn complexes with similar ligands to mL^- in which the ethane

bridge has been replaced by a propane bridge have been obtained and their reactivities towards oxidation are under investigation.

Experimental Section

General remarks: Reagents and solvents were purchased commercially and used as received, except the acetonitrile for electrochemical experiments which was distilled under argon over granular $CaCl_2$.

Caution: Perchlorate salts of metal complexes with organic ligands are potentially explosive. Only small quantities of these compounds should be prepared and they should be handled behind suitable protective shields.

Synthesis of *N,N′*-bis-(2-pyridylmethyl)-*N*-(2-hydroxybenzyl)-*N′*-methyl-ethane-1,2-diamine (mLH): The synthesis of mLH is adapted from the literature[101] and consists of the following two-step synthesis.

Synthesis of N-*(2-hydroxybenzyl)*-N′*-methyl-ethane-1,2-diamine*: *N*-Methyl-ethane-1,2-diamine (0.88 mL, 10 mmol) and salicylaldehyde (1.06 mL, 10 mmol) were stirred in methanol (20 mL) at room temperature for one hour. Methanol (80 mL) was added and the resulting imine was hydrogenated over Pd/C (10%; 60 mg) under pressure (15 bars) overnight. The resulting mixture was filtered over celite, washed with methanol and concentrated under vacuum. A yellow oil (1.54 g, 85% yield) was obtained; ^{1}H NMR (200 MHz, $CDCl_3$): $\delta = 7.15$ (t, 1H, Ar–H), 6.99 (d, 1H, Ar–H), 6.80 (m, 2H, Ar–H), 4.00 (s, 2H, N–CH_2–Ar), 2.75 (s, 4H, N–$(CH_2)_2$–N), 2.43 (s, 3H, CH_3).

Synthesis of N,N′*-bis-(2-pyridylmethyl)*-N-*(2-hydroxybenzyl)*-N′*-methyl-ethane-1,2-diamine*: 2-Picolyl chloride in hydrochloride form (1.85 g, 11 mmol) was dissolved in water (10 mL) and neutralised by 4 M sodium hydroxide. *N*-(2-hydroxybenzyl)-*N′*-methyl-ethane-1,2-diamine (1.0 g, 5.5 mmol) was then added. The resulting mixture was heated to 65°C and neutralised progressively over one hour by addition of small aliquots of 4 M sodium hydroxide in order to prevent the pH value exceeding 9. The mixture was cooled, stirred overnight and then extracted with dichloromethane (6×50 mL). The combined CH_2Cl_2 extracts were washed with water and dried over Na_2SO_4. After concentration under vaccum, a red oil (1.37 g, 69% yield) was obtained and was purified on an alumina column with CH_2Cl_2/MeOH (10:1) as the eluent. The desired compound was isolated as the first product (red oil, 0.60 g, 30% yield); ^{1}H NMR (200 MHz, $CDCl_3$): $\delta = 8.50$ (m, 2H, *H*-C_5H_3N), 7.65–6.70 (m, 10H, *H*-Ar), 3.77 (s, 2H, N–CH_2–C_5H_3N), 3.74 (s, 2H, N–CH_2–C_5H_3N), 3.60 (s, 2H, N–CH_2–C_6H_4OH), 2.73 (dt, 2H, N–CH_2–CH_2), 2.64 (dt, 2H, N–CH_2–CH_2), 2.12 (s, 3H, CH_3).

Synthesis of 1$(ClO_4)_2$: mLH (300 mg, 0.83 mmol)and 2,6-dimethylpyridine (2,6-lutidine; 0.2 mL, 2.0 mmol) in methanol (3 mL) were added to $Mn^{II}(ClO_4)_2 \cdot 6H_2O$ (300 mg, 0.83 mmol) in methanol (3 mL) and the resulting mixture was stirred for 15 min. Distilled water (5 mL) was added to the resulting dark-green solution and a pale-yellow powder precipitated out. The precipitate was filtered, washed with water and carefully dried on a fritted glass to give **1** (330 mg, 38% yield). Crystals suitable for X-ray crystallography were obtained by slow diffusion of diethyl ether in an acetonitrile solution of **1**; IR (KBr): $\tilde{\nu} = 3447$ (w), 2862 (m), 1601 (w), 1570 (m), 1480 (w), 1445 (m), 1267 (w), 1091 (w), 1015 (s), 884 (s), 843 (s), 765 (m), 624 (m), 611 (m), 576 (s), 473 (s) cm^{-1}; elemental analysis: calcd (%) for $C_{44}H_{54}N_8O_{12}Cl_2Mn_2$ (1067.76): C 49.49, H 5.10, N 10.49; found: C 49.56, H 5.02, N 10.17.

Crystallographic data collection and refinement of the structure of [(mL)MnMn(mL)]$(ClO_4)_2$: A colourless crystal with approximate dimensions of 0.20×0.10×0.10 mm was selected. Diffraction collection was carried out on a Nonius diffractometer equipped with a CCD detector. The lattice parameters were determined from ten images recorded with 2° Φ scans and later refined on all data. The data were recorded at 123 K. A 180° Φ range was scanned with 2° steps with the crystal-to-detector distance fixed at 30 mm. Data were corrected for Lorentz polarisation. The structure was solved by direct methods and refined by full-matrix least-squares on F^2 with anisotropic thermal parameters for all non-hydrogen atoms.[102] Hydrogen atoms were introduced at calculated positions as riding atoms, with an isotropic displacement parameter equal to 1.2 (CH_2) or 1.5 (CH_3) times that of the parent atom. The perchlorate anion is found disordered on two positions and refined with a 0.5 occupation factor. All calculations were performed on an O2 Silicon Graphics Station with the SHELXTL package.[103,104]

Formula: $Mn_2C_{44}H_{50}Cl_2N_8O_{10}$; $M_r = 1031.70$, $T = 123(2)$ K, $\lambda = 0.71073$ Å; crystallographic system: orthorhombic; space group: *Fdd2*; $a = 10.954(2)$, $b = 24.052(5)$, $c = 38.982(8)$ Å, $V = 10270(4)$ Å^3, $Z = 8$; $\rho = 1.334$ g cm^{-3}, $\mu = 0.655$ mm^{-1}, $\theta_{max} = 24.73°$; *hkl* ranges: $-12 \le h \le 12$, $-27 \le k \le 28$, $-45 \le L \le 45$; reflections measured: 16010; independent reflections: 4272; reflections observed with $I > 2\sigma(I)$: 3703; parameters: 325; $R1 = 0.0636$ ($R1 = \Sigma||F_o| - |F_c||/\Sigma|F_o|$); $wR2 = 0.1664$ ($wR2 = \{\Sigma[w(F_o^2 - F_c^2)^2]^2/\Sigma[w(F_o^2)^2]^2\}^{1/2}$ with $w = 1/[\sigma^2(F_o^2) + (0.1000P)^2]$, where $P = (F_o^2 + 2F_c^2)/3$); $(\Delta/\sigma)_{max} = 0.020$, $\Delta\rho_{max} = 0.610$ e Å^{-3}, $\Delta\rho_{min} = -0.379$ e Å^{-3}.

CCDC-215363 contains the supplementary crystallographic data (excluding structures factors) for this paper. These data can be obtained free of charge via www.ccdc.cam.ac.uk/conts/retreiving.html (or from Cambridge Crystallographic Data Centre, 12 Union Road, Cambridge CB2 1EZ, UK; fax: (+44) 1223–336–033; or e-mail: deposit@ccdc.cam.ca.uk).

Physical measurements: Elemental analyses were performed at Service Central d'Analyses, CNRS Vernaison-France. Infrared spectra were recorded on KBr pellets over the range 4000–200 cm^{-1} with a Perkin–Elmer Spectrum 1000 spectrophotometer. ^{1}H NMR spectra were recorded by using a Bruker AC-200 (200 MHz) or a Bruker AM-250 (250 MHz) apparatus.

Magnetic susceptibility measurements: Magnetic susceptibility data were recorded on an MPMS5 magnetometer (Quantum Design). The calibration was made at 298 K by using a palladium reference sample furnished by Quantum Design. The data were collected over a temperature range of 2–300 K at a magnetic field of 10 kOe and were corrected for diamagnetism. The $\chi_M T$ versus T curves were fitted by using the van Vleck formula and assuming the same g factor for each S spin state. The total spin, S, runs from $|S_1 - S_2|$ to $(S_1 + S_2)$ by unit steps. The exchange Hamiltonian used was $\hat{H} = -J\hat{S}_1\hat{S}_2$, in which J stands for the exchange coupling constant and $\hat{S}_1$ and $\hat{S}_2$ for the spin operators associated with the electronic spin of the Mn^{II} sites ($S_1 = S_2 = 5/2$).

EPR spectroscopy: EPR spectra were recorded on a Bruker 200D (X band) and Bruker ELEXSYS 500 (X and Q band) spectrometer equipped with an Oxford Instrument continuous-flow liquid helium cryostat and a temperature-control system. Solution spectra were recorded with 0.1 M tetrabutylammonium perchlorate in acetonitrile as solvent.

Quantification at X band of the mixed-valent di-μ-oxo $Mn^{III}Mn^{IV}$ system was performed by using the di-μ-oxo complex $[(mL_4)Mn^{III}(\mu\text{-}O)_2\text{-}Mn^{IV}(mL_4)]^{3+}$ as a reference. The X-band EPR solution spectrum of 0.1 mM $[(mL_4)Mn^{III}(\mu\text{-}O)_2\text{-}Mn^{IV}(mL_4)](BPh_4)_2(ClO_4)$[36] was recorded at both 20 and 100 K. The spectra were superimposable, a fact demonstrating that the signal only originates from the $S = 1/2$ ground state at 100 K. Nonsaturating recording conditions were only achieved at 100 K.

Simulations of the X-band EPR spectra were performed by using a program described in ref. [57]. An $S = 1/2$ system was considered and the EPR spectrum profile was assumed to be governed by the Zeeman effect within the $S = 1/2$ state and the two hyperfine interactions between the $S = 1/2$ electronic spin on one hand and each manganese $I = 5/2$ nuclear spin on the other. The Hamiltonian [Eq. (3)] was used with assumption of colinear tensors.

$$\hat{H} = \mu_B \hat{B}\tilde{g}\hat{S} + \hat{S}\tilde{A}_1\hat{I}_1 + \hat{S}\tilde{A}_2\hat{I}_2 \qquad (3)$$

Only the electronic and nuclear spin values are introduced to perform the EPR simulation and no hypothesis was formulated on the oxidation states of the manganese ions. A Gaussian line shape was used.

Cyclic voltammetry and bulk electrolysis: Cyclic voltammetry and chronocoulometry measurements were recorded with an EGG PAR potentiostat (M273 model). The counterelectrode was an Au wire, the working electrode was a glassy carbon disc carefully polished before measurement of each voltammogram with a 1 μm diamond paste, sonicated in ethanol bath and then washed carefully with ethanol. In absence of such treatment of the working electrode surface, the successive cyclic voltammograms were not reproducible. The reference electrode was an $Ag/AgClO_4$

electrode (0.530 V versus the normal hydrogen electrode) isolated in a fritted bridge. The solvent used was distilled acetonitrile where tetrabutylammonium perchlorate was added to obtain a 0.1 M supporting electrolyte when the experiments are carried out at room temperature or a 0.2 M supporting electrolyte for experiments carried out at low temperature (below 10 °C). Low-temperature regulation was insured by a Julabo circulation cryostat.

UV/Vis spectroscopy: UV/Vis spectra were recorded on a Varian Cary 300 Bio or a Varian Cary 5E spectrophotometer at 20 °C with either 0.1 or 1 cm quartz cuvettes.

UV/Vis spectroelectrochemistry: Spectra were recorded on a Varian Cary 5E spectrophotometer by using a thin-layer cell with a 0.5-mm optical pathlength. The working electrode was a platinum grid (0.3 mm). Reference and counterelectrodes were identical to those used for the cyclic voltametry experiments.

Mass spectrometry: All experiments were performed on an electrospray triple-quadripole API 2000 apparatus (Applied Biosystems). Some applied parameters were unchanged for all experiments, such as the voltage applied on the counterelectrode (5000 V), the pressure of the curtain gas (20 psi) and the declustering potential (20 V). No heating source was used (ambient temperature). For infused solutions, the complexes were analysed in positive ion mode. Diluted samples ($\approx 10^{-3}$ M) in pure acetonitrile were infused into the electrospray ionisation source at a flow rate of 7 $\mu L\,min^{-1}$.

Acknowledgement

We are grateful to Dr. Alain Boussac (Service de Bioénergétique, URA CNRS 2096, CEA Saclay, Gif-sur-Yvette, France) for EPR facilities and to Dr. Marie-Noëlle Collomb and Pr. Jean-Jacques Girerd for stimulating discussions. We thank the Conseil Régional de l'Ile de France for its contribution to the acquisition of the Bruker ELEXSYS X- and Q-band EPR spectrometer. The COST D21 European action and the LRC-CEA project are acknowledged for their financial support.

[1] E. J. Larson, V. L. Pecoraro, *Manganese Redox Enzymes*, **1992**, 1–28.
[2] J. D. Crowley, D. A. Traynor, D. C. Weatherburn, *Met. Ions Biol. Syst.* **2000**, *37*, 209–278.
[3] G. C. Dismukes, *Chem. Rev.* **1996**, *96*, 2909–2926.
[4] D. W. Yoder, J. Hwang, J. E. Penner-Hahn, *Met. Ions Biol. Syst.* **2000**, *37*, 527–557.
[5] Z. F. Kanyo, L. R. Scolnick, D. E. Ash, D. W. Christianson, *Nature* **1996**, *383*, 554–557.
[6] W. Oehlmann, U. Griepenburg, G. Auling, *Biotechnol. Lett.* **1998**, *20*, 483–488.
[7] Abbreviations: OEC = oxygen-evolving complex; mLH = *N*,*N*′-bis(2-pyridylmethyl)-*N*-(2-hydroxybenzyl)-*N*′-methylethane-1,2-diamine; H_2BBPEN = *N*,*N*′-bis(2-hydroxybenzyl)-*N*,*N*′-bis(2-pyridylmethyl)ethane-1,2-diamine; mL_5 = *N*,*N*,*N*′-tris(2-pyridylmethyl)-*N*′-methylethane-1,2-diamine; mL_4 = *N*,*N*′-bis(2-pyridylmethyl)-*N*,*N*′-dimethylethane-1,2-diamine; m_1L_4 = *N*,*N*′-bis(2-pyridylmethyl)-*N*-methylethane-1,2-diamine; N,Nbispicen = *N*,*N*-bis(2-pyridylmethyl)-ethane-1,2-diamine; L_4 = *N*,*N*′-bis-(2-pyridylmethyl)ethane-1,2-diamine.
[8] R. J. Debus, *Biochim. Biophys. Acta* **1992**, *1102*, 269–352.
[9] V. K. Yachandra, K. Sauer, M. P. Klein, *Chem. Rev.* **1996**, *96*, 2927–2950.
[10] J. Nugent, *Biochim. Biophys. Acta* **2001**, *1503*, 1–259.
[11] C. Goussias, A. Boussac, A. W. Rutherford, *Philos. Trans. R. Soc. London Ser. B* **2002**, *357*, 1369–1381.
[12] V. K. Yachandra, *Philos. Trans. R. Soc. London Ser. B* **2002**, *357*, 1347–1358.
[13] B. Kok, B. Forbush, M. Mcgloin, *Photochem. Photobiol.* **1970**, *11*, 457–475.
[14] A. Zouni, H.-T. Witt, J. Kern, P. Fromme, N. Krauß, W. Saenger, P. Orth, *Nature* **2001**, *409*, 739–743.
[15] N. Kamiya, J.-R. Shen, *Proc. Natl. Acad. Sci. USA* **2003**, *100*, 98–103.
[16] A. W. Rutherford, P. Faller, *Trends Biochem. Sci.* **2001**, *26*, 341–344.
[17] J. E. Penner-Hahn, *Struct. Bonding* **1998**, *90*, 1–36.
[18] J. H. Robblee, R. M. Cinco, V. K. Yachandra, *Biochim. Biophys. Acta* **2001**, *1503*, 7–23.
[19] G. C. Dismukes, Y. Siderer, *Proc. Natl. Acad. Sci. USA* **1981**, *78*, 274–278.
[20] J. Messinger, J. H. Robblee, W. O. Yu, K. Sauer, V. K. Yachandra, M. P. Klein, *J. Am. Chem. Soc.* **1997**, *119*, 11349–11350.
[21] J. M. Peloquin, R. D. Britt, *Biochim. Biophys. Acta* **1992**, *1102*, 269–352.
[22] T. G. Carrell, A. M. Tyryshkin, G. C. Dismukes, *J. Biol. Inorg. Chem.* **2002**, *7*, 2–22.
[23] V. J. DeRose, E. Mukerji, M. J. Latimer, V. K. Yachandra, K. Sauer, M. P. Klein, *J. Am. Chem. Soc.* **1994**, *116*, 5239–5249.
[24] V. K. Yachandra, V. J. DeRose, M. J. Latimer, E. Mukerji, K. Sauer, M. P. Klein, *Science* **1993**, *260*, 675–679.
[25] K. Hasegawa, T.-A. Ono, Y. Inoue, M. Kusunoki, *Bull. Chem. Soc. Jpn.* **1999**, *72*, 1013–1023.
[26] K. Hasegawa, T.-A. Ono, Y. Inoue, M. Kusunoki, *Chem. Phys. Lett.* **1999**, *300*, 9–19.
[27] M. Zheng, G. C. Dismukes, *Inorg. Chem.* **1996**, *35*, 3307–3319.
[28] D. W. Randall, B. E. Sturgeon, J. A. Ball, G. A. Lorigan, M. K. Chan, M. P. Klein, W. H. Armstrong, R. D. Britt, *J. Am. Chem. Soc.* **1995**, *117*, 11780–11789.
[29] C. Philouze, G. Blondin, J.-J. Girerd, J. Guilhem, C. Pascard, D. Lexa, *J. Am. Chem. Soc.* **1994**, *116*, 8557–8565.
[30] K. Wieghardt, *Angew. Chem.* **1994**, *106*, 765–768 Angew. Chem. Int. Ed. Engl. **1994**, *33*, 725–728.
[31] N. A. Law, M. T. Caudle, V. L. Pecoraro, *Adv. Inorg. Chem.* **1998**, *46*, 305–440.
[32] V. L. Pecoraro, W.-Y. Hsieh, *Met. Ions Biol. Syst.* **2000**, *37*, 429–504.
[33] Y.-M. Frapart, A. Boussac, R. Albach, E. Anxolabéhère-Mallart, M. Delroisse, J.-B. Verlach, G. Blondin, J.-J. Girerd, J. Guilhem, M. Cesario, A. W. Rutherford, D. Lexa, *J. Am. Chem. Soc.* **1996**, *118*, 2669–2678.
[34] O. Horner, E. Anxolabéhère-Mallart, M.-F. Charlot, L. Tchertanov, J. Guilhem, T. A. Mattioli, A. Boussac, J.-J. Girerd, *Inorg. Chem.* **1999**, *38*, 1222–1232.
[35] J. Glerup, P. A. Goodson, A. Hazell, R. Hazell, D. J. Hodgson, C. J. McKenzie, K. Michelsen, U. Rychlewska, *Inorg. Chem.* **1994**, *33*, 4105–4111.
[36] C. Hureau, G. Blondin, M. Cesario, S. Un, *J. Am. Chem. Soc.* **2003**, *125*, 11637–11645.
[37] O. Horner, M.-F. Charlot, A. Boussac, E. Anxolabéhère-Mallart, L. Tchertanov, J. Guilhem, J.-J. Girerd, *Eur. J. Inorg. Chem.* **1998**, 721–727.
[38] B. C. Dave, R. S. Czernuszewicz, M. R. Bond, C. J. Carrano, *Inorg. Chem.* **1993**, *32*, 3593–3594.
[39] S. Pal, J. W. Gohdes, W. C. A. Wilisch, W. H. Armstrong, *Inorg. Chem.* **1992**, *31*, 713–716.
[40] S. Pal, M. K. Chan, W. H. Armstrong, *J. Am. Chem. Soc.* **1992**, *114*, 6398–6406.
[41] S. Pal, M. M. Olmstead, R. N. Armstrong, *Inorg. Chem.* **1995**, *34*, 4708–4715.
[42] K. Wieghardt, U. Bossek, L. Zsolnai, G. Huttner, G. Blondin, J.-J. Girerd, F. Babonneau, *J. Chem. Soc. Chem. Commun.* **1987**, 651–653.
[43] T. K. Lal, R. Mukherjee, *Inorg. Chem.* **1998**, *37*, 2373–2382.
[44] M. U. Triller, W.-Y. Hsieh, V. L. Pecoraro, A. Rompel, B. Krebs, *Inorg. Chem.* **2002**, *41*, 5544–5554.
[45] J. E. Sheats, R. S. Czernuszewicz, G. C. Dismukes, A. L. Rheingold, V. Petrouleas, J. Stubbe, W. H. Armstrong, R. H. Beer, S. J. Lippard, *J. Am. Chem. Soc.* **1987**, *109*, 1435–1444.
[46] J. B. Vincent, H.-L. Tsai, A. G. Blackman, S. Wang, P. D. W. Boyd, K. Folting, J. C. Huffman, E. B. Lobkovsky, D. N. Hendrickson, G. Christou, *J. Am. Chem. Soc.* **1993**, *115*, 12353–12361.
[47] S. K. Mandal, R. N. Armstrong, *Inorg. Chim. Acta* **1995**, *229*, 261–270.

[48] K. Wieghardt, U. Bossek, D. Ventur, J. Weiss, *J. Chem. Soc. Chem. Commun.* **1985**, 347–349.
[49] K. Wieghardt, U. Bossek, J. Bonvoisin, P. Beauvillain, J.-J. Girerd, B. Nuber, J. Weiss, J. Heinze, *Angew. Chem.* **1986**, *98*, 1026–1027; *Angew. Chem. Int. Ed. Engl.* **1986**, *25*, 1030–1031.
[50] C. A. Kipke, M. J. Scott, J. W. Gohdes, W. H. Armstrong, *Inorg. Chem.* **1990**, *29*, 2193–2194.
[51] R. F. Ziolo, R. H. Stanford, G. R. Rossman, H. B. Gray, *J. Am. Chem. Soc.* **1974**, *96*, 7910–7915.
[52] L. H. Vogt, A. Zalkin, D. H. Templeton, *Inorg. Chem.* **1967**, *6*, 1725–1730.
[53] N. Kitajima, M. Osawa, M. Tanaka, Y. Moro-Oka, *J. Am. Chem. Soc.* **1991**, *113*, 8952–8953.
[54] M. K. Chan, W. H. Armstrong, *J. Am. Chem. Soc.* **1989**, *111*, 9121–9122.
[55] C. Baffert, M.-N. Collomb, A. Deronzier, J. Pécaut, J. Limburg, R. H. Crabtree, G. W. Brudvig, *Inorg. Chem.* **2002**, *41*, 1404–1411.
[56] C. Baffert, M.-N. Collomb, A. Deronzier, S. Kjaergaard-Knudsen, J.-M. Latour, K. H. Lund, C. J. McKenzie, M. Mortensen, L. P. Nielsen, N. Thorup, *J. Chem. Soc. Dalton Trans.* **2003**, 1765–1772.
[57] M. J. Camenzind, B. C. Schardt, C. L. Hill, *Inorg. Chem.* **1984**, *23*, 1984–1986.
[58] J. Bonvoisin, G. Blondin, J.-J. Girerd, J.-L. Zimmermann, *Biophys. J.* **1992**, *61*, 1076–1086.
[59] G. Blondin, R. Davydov, C. Philouze, M.-F. Charlot, S. Styring, B. Åkermark, J.-J. Girerd, A. Boussac, *J. Chem. Soc. Dalton Trans.* **1997**, 4069–4074.
[60] K.-O. Schäfer, R. Bittl, W. Zweygart, F. Lendzian, G. Haselhorst, T. Weyhermüller, K. Wieghardt, W. Lubitz, *J. Am. Chem. Soc.* **1998**, *120*, 13104–13120.
[61] K.-O. Schäfer, R. Bittl, F. Lendzian, V. V. Barynin, T. Weyhermüller, K. Wieghardt, W. Lubitz, *J. Phys. Chem. B* **2003**, *107*, 1242–1250.
[62] C. Policar, M. Knüpling, Y.-M. Frapart, S. Un, *J. Phys. Chem. B* **1998**, *102*, 10391–10398.
[63] S. R. Cooper, G. C. Dismukes, M. P. Klein, M. Calvin, *J. Am. Chem. Soc.* **1978**, *100*, 7248–7252.
[64] P. A. Goodson, J. Glerup, D. J. Hodgson, E. Michelsen, E. Pedersen, *Inorg. Chem.* **1990**, *29*, 503–508.
[65] K. Wieghardt, U. Bossek, B. Nuber, J. Weiss, J. Bonvoisin, M. Corbella, S. E. Vitols, J.-J. Girerd, *J. Am. Chem. Soc.* **1988**, *110*, 7398–7411.
[66] C. Hureau, E. Anxolabéhère-Mallart, M. Nierlich, F. Gonnet, E. Rivière, G. Blondin, *Eur. J. Inorg. Chem.* **2002**, 2710–2719.
[67] D. P. Kessissoglou, W. M. Butler, V. L. Pecoraro, *Inorg. Chem.* **1987**, *26*, 495–503.
[68] E. Gallo, E. Solari, N. Re, C. Floriani, A. Chiesi-Villa, C. Rizzoli, *J. Am. Chem. Soc.* **1997**, *119*, 5144–5154.
[69] D. Coucouvanis, K. Greiwe, A. Salifoglou, P. Challen, A. Simopoulos, A. Kostikas, *Inorg. Chem.* **1988**, *27*, 593–594.
[70] T. C. Higgs, K. Spartalian, C. J. O'Connor, B. F. Matzanke, C. J. Carrano, *Inorg. Chem.* **1998**, *37*, 2263–2272.
[71] T. Howard, J. Telser, V. J. DeRose, *Inorg. Chem.* **2000**, *39*, 3379–3385.
[72] I. Romero, M.-N. Collomb, A. Deronzier, A. Llobet, E. Perret, J. Pécaut, L. Le Pape, J.-M. Latour, *Eur. J. Inorg. Chem.* **2001**, 69–72.
[73] H. Adams, N. A. Bailey, N. Debaeker, D. E. Fenton, W. Kanda, J.-M. Latour, H. Okawa, H. Sakiyama, *Angew. Chem.* **1995**, *107*, 2749–2751; *Angew. Chem. Int. Ed. Engl.* **1995**, *34*, 2535–2537.
[74] B. Albela, M. Corbella, J. Ribas, I. Castro, J. Sletten, H. Stoeckli-Evans, *Inorg. Chem.* **1998**, *37*, 788–798.
[75] E. J. Laskowski, D. N. Hendrickson, *Inorg. Chem.* **1978**, *17*, 457–470.
[76] S. V. Khangulov, P. J. Pessiki, V. V. Barynin, D. E. Ash, G. C. Dismukes, *Biochemistry* **1995**, *34*, 2015–2025.
[77] A. E. Meier, M. M. Whittaker, J. W. Whittaker, *Biochemistry* **1996**, *35*, 348–360.
[78] B. S. Antharavally, R. R. Poyner, P. W. Ludden, *J. Am. Chem. Soc.* **1998**, *120*, 8897–8898.
[79] S. Blanchard, G. Blain, E. Rivière, M. Nierlich, G. Blondin, *Chem. Eur. J.* **2003**, *9*, 4260–4268.
[80] S. Blanchard, G. Blondin, E. Rivière, M. Nierlich, J.-J. Girerd, *Inorg. Chem.* **2003**, *42*, 4568–4578.
[81] A. Bencini, D. Gatteschi, *EPR of Exchange Coupled Systems*, Springer, Berlin, **1990**.
[82] A. Neves, S. M. D. Erthal, I. Vencato, A. S. Ceccato, Y. P. Mascarenhas, O. R. Nascimento, M. Hörner, A. A. Batista, *Inorg. Chem.* **1992**, *31*, 4749–4755.
[83] P. A. Goodson, J. Glerup, D. J. Hodgson, K. Michelsen, H. Weihe, *Inorg. Chem.* **1991**, *30*, 4909–4914.
[84] A. L. Nivorozhkin, E. Anxolabéhère-Mallart, P. Mialane, R. Davydov, J. Guilhem, M. Cesario, J.-P. Audière, J.-J. Girerd, S. Styring, L. Schussler, J.-L. Seris, *Inorg. Chem.* **1997**, *36*, 846–853.
[85] U. Auerbach, T. Weyhermüller, K. Wieghardt, B. Nuber, E. Bill, C. Butzlaff, A. Trautwein, *Inorg. Chem.* **1993**, *32*, 508–519.
[86] M. J. Baldwin, T. L. Stemmler, P. J. Riggs-Gelasco, M. L. Kirk, J. E. Penner-Hahn, V. L. Pecoraro, *J. Am. Chem. Soc.* **1994**, *116*, 11349–11356.
[87] P. A. Goodson, J. Glerup, D. J. Hodgson, K. Michelsen, H. Weihe, *Inorg. Chem.* **1991**, *30*, 4909–4914.
[88] K. J. Brewer, M. Calvin, R. S. Lumpkin, J. W. Otvos, L. O. Spreer, *Inorg. Chem.* **1989**, *28*, 4446–4451.
[89] J. Simaan, S. Poussereau, G. Blondin, J.-J. Girerd, D. Defaye, C. Philouze, J. Guilhem, L. Tchertanov, *Inorg. Chim. Acta* **2000**, *299*, 221–230.
[90] Y. Gultneh, T. B. Yisgedu, Y. T. Tesema, R. J. Butcher, *Inorg. Chem.* **2003**, *42*, 1857–1867.
[91] O. Horner, J.-J. Girerd, C. Philouze, L. Tchertanov, *Inorg. Chim. Acta* **1999**, *290*, 139–144.
[92] Y. Ikawa, T. Nagata, K. Maruyama, *Chem. Lett.* **1993**, 1049–1052.
[93] The irreversible deprotonation of $[(mL)Mn^{III}(OH_2)]^{2+}$ thus favours the dissociation of the dinuclear mixed-valent $[(mL)Mn^{II}$-$Mn^{III}(mL)]^{3+}$ into Mn^{II} and Mn^{III} mononuclear complexes and consequently increases the concentration of monomeric species near the electrode. With the oxidation potential of the monomeric Mn^{II} species being close to that of **1**, its oxidation contributes to the intensity of peak 1.
[94] Intermediate UV/Vis spectra were not systematically recorded during the course of the electrolysis. Nevertheless, a transitory pink colour was observed and the corresponding electronic spectrum displayed a large band at 500 nm similar to the one reported for species **2**.
[95] M.-N. Collomb Dunand-Sauthier, A. Deronzier, I. Romero, *J. Electroanal. Chem.* **1997**, *436*, 219–225.
[96] M.-N. Collomb Dunand-Sauthier, A. Deronzier, A. Piron, X. Pradon, S. Ménage, *J. Am. Chem. Soc.* **1998**, *120*, 5373–5380.
[97] K. Srinivasan, P. Michaud, J. K. Kochi, *J. Am. Chem. Soc.* **1986**, *108*, 2309–2320.
[98] D. Feichtinger, D. A. Plattner, *Angew. Chem.* **1997**, *109*, 1796–1798; *Angew. Chem. Int. Ed. Engl.* **1997**, *36*, 1718–1719.
[99] D. Feichtinger, D. A. Plattner, *Chem. Eur. J.* **2001**, *7*, 591–599.
[100] E. J. Larson, V. L. Pecoraro, *J. Am. Chem. Soc.* **1991**, *113*, 3810–3818.
[101] S. Ito, Y. Ishikawa, S. Nishino, T. Kobayashi, S. Ohba, Y. Nishida, *Polyhedron* **1998**, *17*, 4379–4391.
[102] G. M. Sheldrick, *Acta Crystallogr. Sect. A* **1990**, *46*, 467.
[103] G. M. Sheldrick, SHELXTL-97, program for the refinement of crystal structures, University of Göttingen, Germany, **1997**.
[104] G. M. Sheldrick, SHELXTL, Version 5.1, University of Göttingen, Germany, distributed by Bruker AXS, Madison, WI, **1999**.

Received: September 4, 2003 [F5515]